Electronic Supplementary Information

Nb_2O_5-Ni_3N heterojunction tuned by interface oxygen vacancy engineering for enhancement of electrocatalytic hydrogen evolution activity

Xiao Hui Chen,[a] Xiao Lin Li,[a] Li Li Wu,[a] Hong Chuan Fu,[a] Juan Luo,[a] Li Shen,[a] Qing Zhang,[a] Jing Lei Lei,[b] Hong Qun Luo*[a] and Nian Bing Li*[a]

[a] *School of Chemistry and Chemical Engineering, Southwest University, Chongqing 400715, People's Republic of China*

[b] *School of Chemistry and Chemical Engineering, Chongqing University, Chongqing 400044, People's Republic of China*

*Corresponding author.

Hong Qun Luo and Nian Bing Li

E-mail address: luohq@swu.edu.cn; linb@swu.edu.cn

Material

Ni foam (NF) was obtained from Cyber Electrochemistry (Beijing, China). Ammonium niobate(V)oxalate hydrate ($C_2H_2O_4 \cdot xNH_3 \cdot xNb$), oxalic acid ($H_2C_2O_4$), and urea ($CO(NH_2)_2$) were purchased from Aladdin Co., Ltd. (Shanghai, China). Pt/C (20 wt % Pt on Vulcan XC-72R), and Nafion (5 wt %) were purchased from Sigma-Aldrich Chemical Reagent Co., Ltd. (USA). Potassium hydroxide (KOH) was produced from Chuandong Chemical Co., Ltd. (Chengdu, China). All chemicals were used as received without further purification.

Characterization

The morphology of the obtained materials was observed by scanning electron microscopy (SEM, ZEISS Gemini 300, ZEISS, Germany) and transmission electron microscopy (TEM, Tecnai G220, Fei Corporation, Japan). The crystalline structures of samples were identified by powder X-ray diffraction (XRD, X' Pert PRO, PANalytical B.V., Holland) using Cu-Kα radiation. The Raman spectra were measured on a Horiba Scientific LabRAM HR Evolution (HORIBA Jobin Yvon, France). The X-ray photoelectron spectroscopy (XPS) analysis was measured on Thermo Scientific K-Alpha using Mg-Kα radiation (Thermoelectricity Instruments, USA).

Electrochemical characterization

Electrochemical characterizations were conducted using a CHI 660E electrochemical workstation with a three-electrode cell in 1.0 M KOH electrolyte. A graphite rod and Ag/AgCl (KCl saturated) was used as the counter and reference electrode, respectively. Nb_2O_5-Ni_3N/NF (0.5 cm^2) served directly as the working electrode. Linear sweep voltammetry (LSV) for HER was performed at a scan rate of 5 mV s^{-1}. Electrochemical impedance spectroscopy (EIS) was carried out in the frequency range of 10^{-1} to 10^5 Hz, with an amplitude of 5 mV at an overpotential of 127 mV. Under these parameters, the Nyquist plots of the Nb_2O_5-Ni_3N/NF can form a relatively complete semicircle. All the polarization curves tested in the three-electrode cell were without *iR*-correction without special instructions. The stability test was conducted at the current density of -10, -50, -100, and -200 mA cm^{-2} for 12 h by chronoamperometric measurement, respectively. The Tafel slopes were calculated by the Tafel equation ($\eta = b \log j + a$, where η is the overpotential, b is the Tafel slope, and j is the current density normalized by geometric area). The electrochemical surface area (ECSA) of the as-prepared materials was estimated from their C_{dl}, which has been measured using simple cyclic voltammetry method. Here the potential window has been chosen outside the possible Faradic region of the material. Then the current is only generated for charging of double layer which is expected to have a linear relationship with the active surface area. The relationship between the capacitive current density, Δj ($\Delta j = (j_{anodic}-j_{cathodic})/2$) at 0.27 V vs. RHE), and the scan rate is linear and the double layer capacitance (C_{dl}) has been calculated from the slope. The measured potentials were normalized to reversible hydrogen electrode (RHE) based on the Nernst equation E(RHE) = E(Ag/AgCl) + 0.0591 × pH + 0.197.

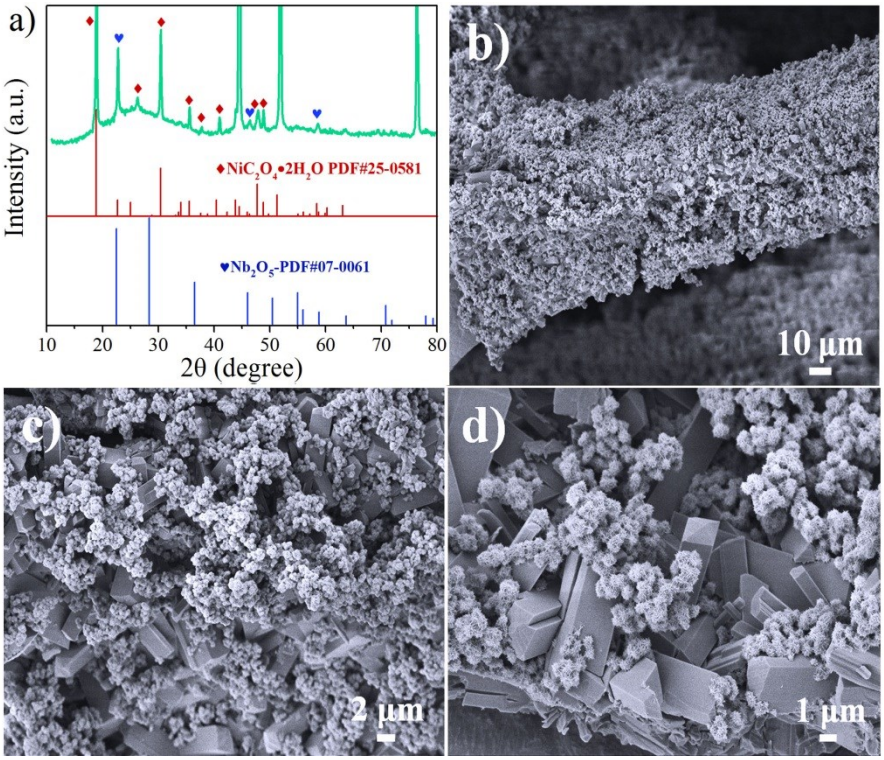

Fig. S1. a) XRD pattern and b-d) SEM images of Nb_2O_5-NiC_2O_4.

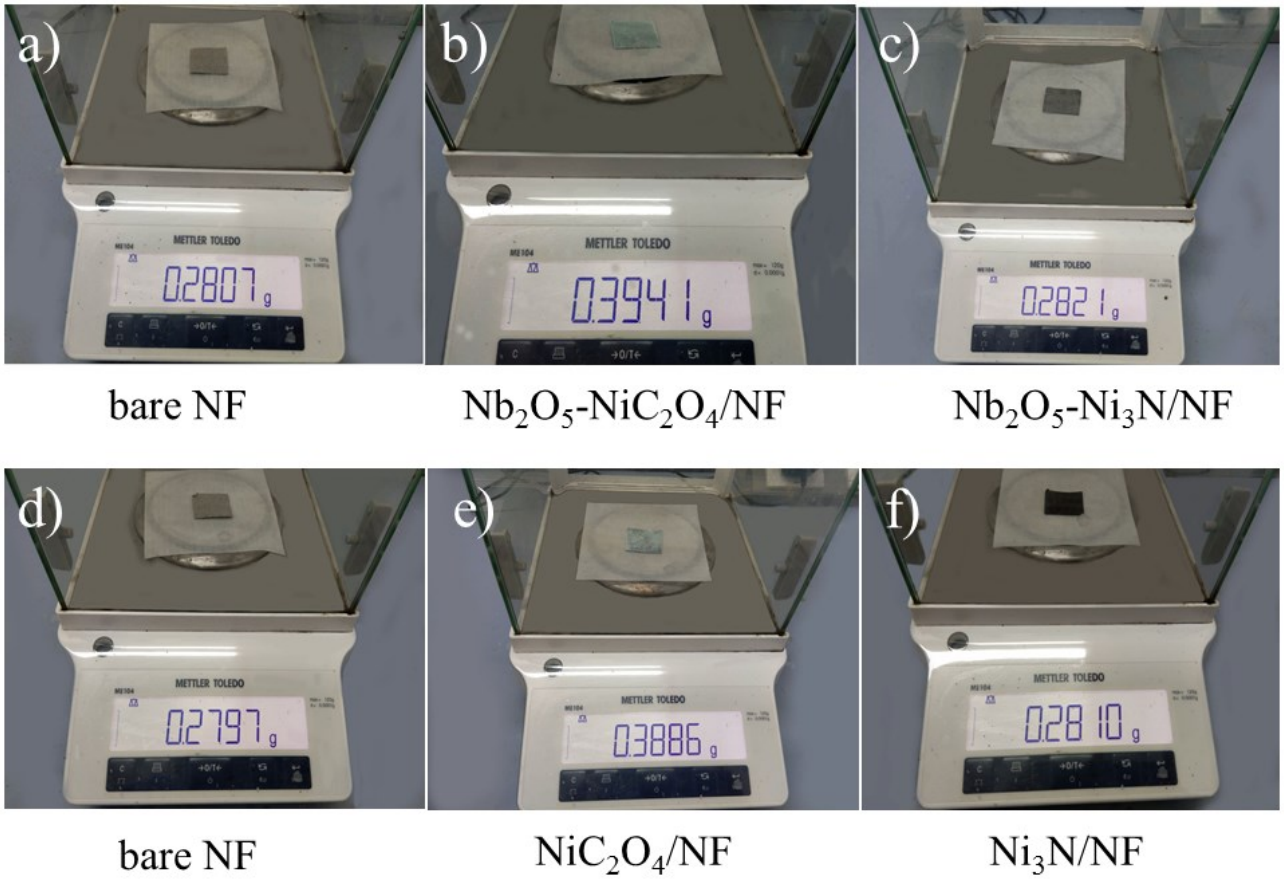

Fig. S2. The mass of a) bare NF (m_1, 0.2807 g), b) Nb_2O_5-NiC_2O_4/NF (m_2, 0.3941 g), c) Nb_2O_5-Ni_3N/NF (m_3, 0.2821 g), d) another piece of NF (m_4, 0.2797 g), e) NiC_2O_4/NF (m_5, 0.3886 g), and Ni_3N/NF (m_6, 0.2810 g).

The loading mass (Δm_1) of Nb_2O_5-Ni_3N on NF is calculated as follows:

$$\Delta m_1 = (m_3 - m_1)/A \quad (1)$$

The loading mass (Δm_2) of Ni_3N on NF is calculated as follows:

$$\Delta m_2 = (m_6 - m_4)/A \quad (2)$$

where A is the area of NF (A = 3 cm × 3 cm).

The loading masses of Nb_2O_5- Ni_3N and Ni_3N on NF are 0.16 and 0.14 mg/cm^2, respectively.

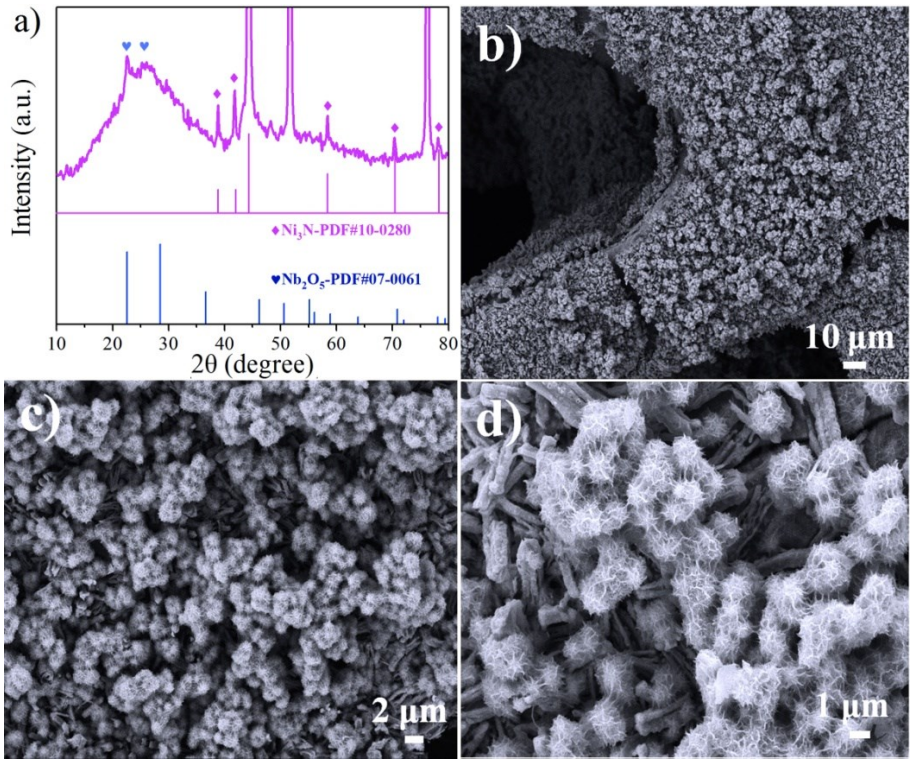

Fig. S3. a) XRD pattern and b-d) SEM images of Nb_2O_5-Ni_3N.

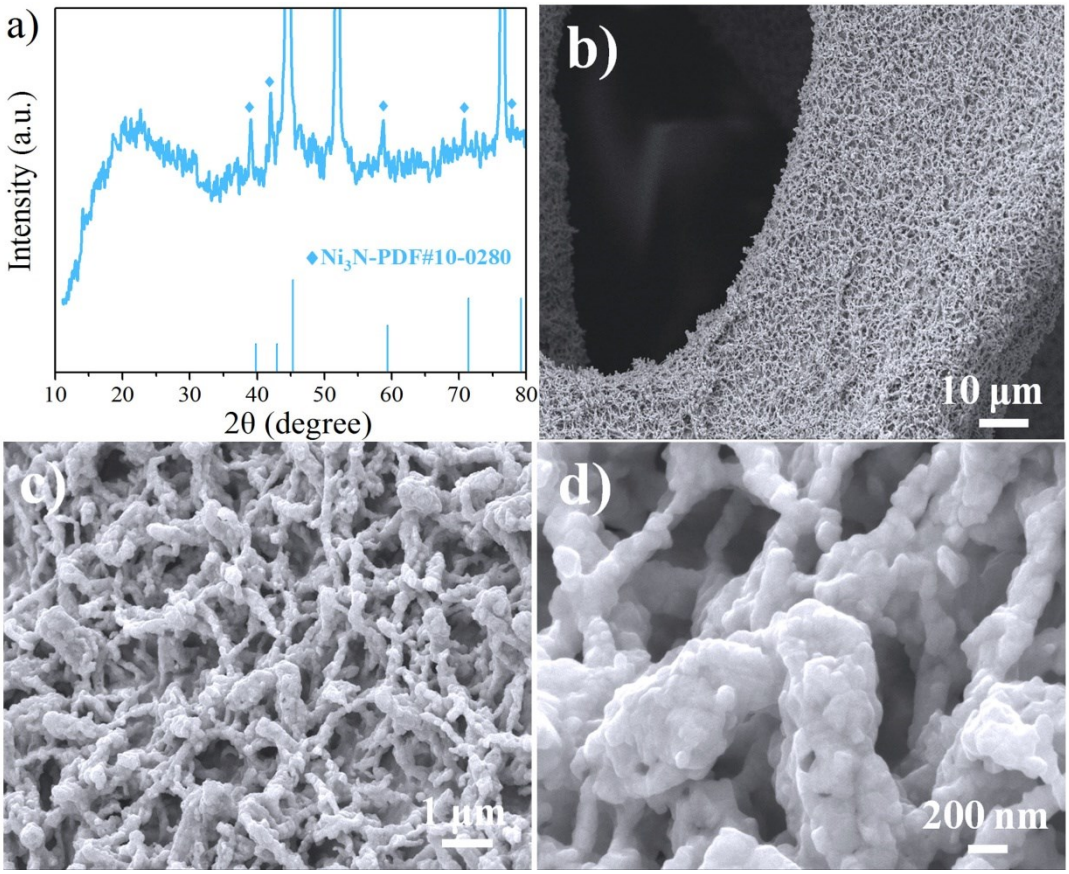

Fig. S4. a) XRD pattern and b-d) SEM images of Ni_3N.

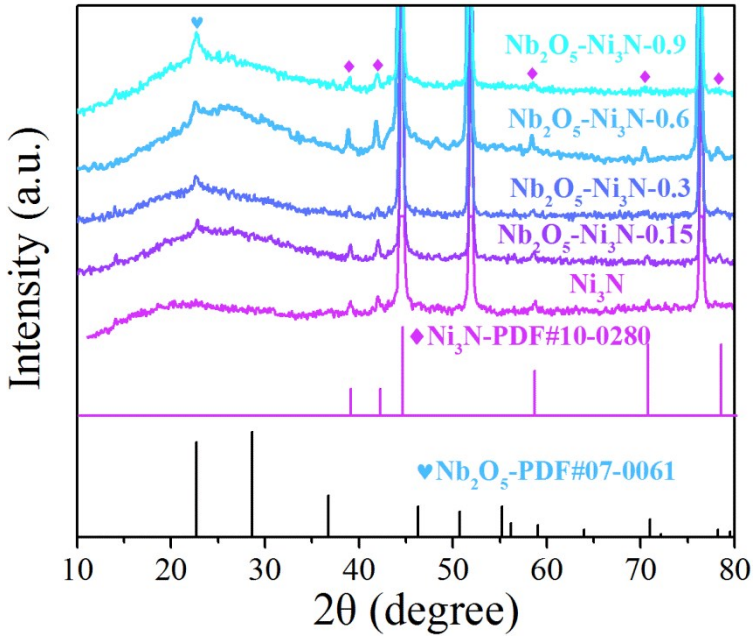

Fig. S5. XRD patterns of Ni_3N, Nb_2O_5-Ni_3N-0.15, Nb_2O_5-Ni_3N-0.3, Nb_2O_5-Ni_3N-0.6 and Nb_2O_5-Ni_3N-0.9.

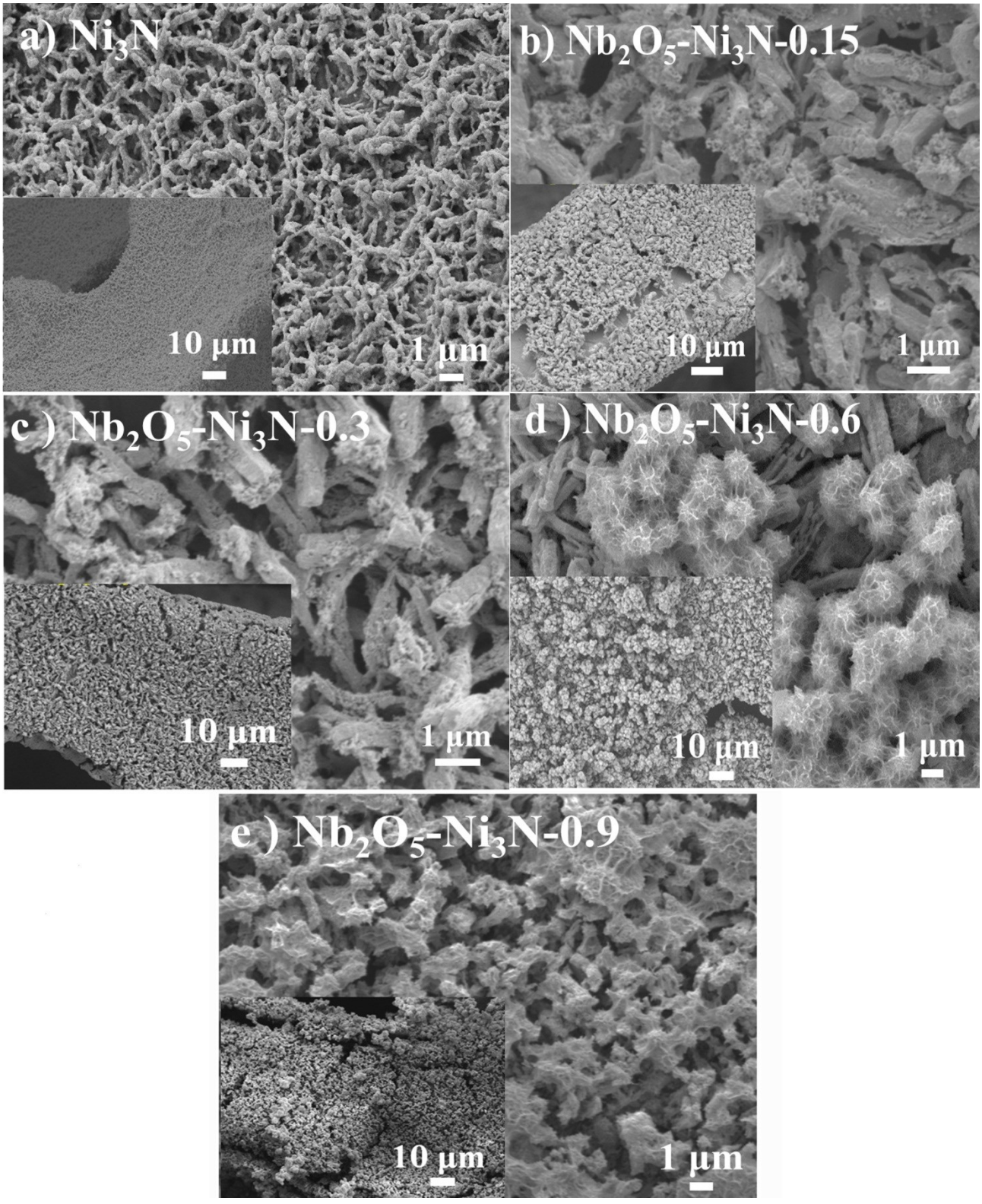

Fig. S6. SEM images of a) Ni_3N, b) Nb_2O_5-Ni_3N-0.15, c) Nb_2O_5-Ni_3N-0.3, d) Nb_2O_5-Ni_3N-0.6 and e) Nb_2O_5-Ni_3N-0.9.

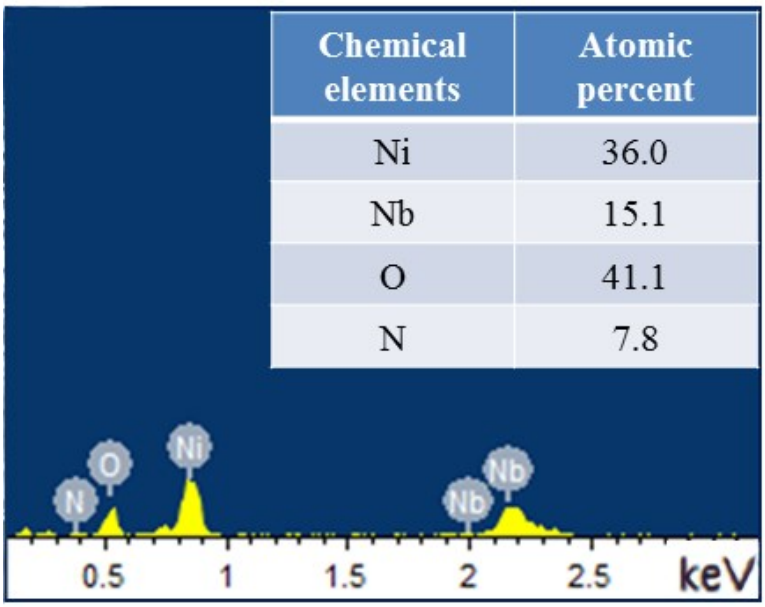

Fig. S7. EDX data of Nb_2O_5-Ni_3N. The Nb_2O_5-Ni_3N mentioned in this work refers to Nb_2O_5-Ni_3N-0.6 without otherwise indicated.

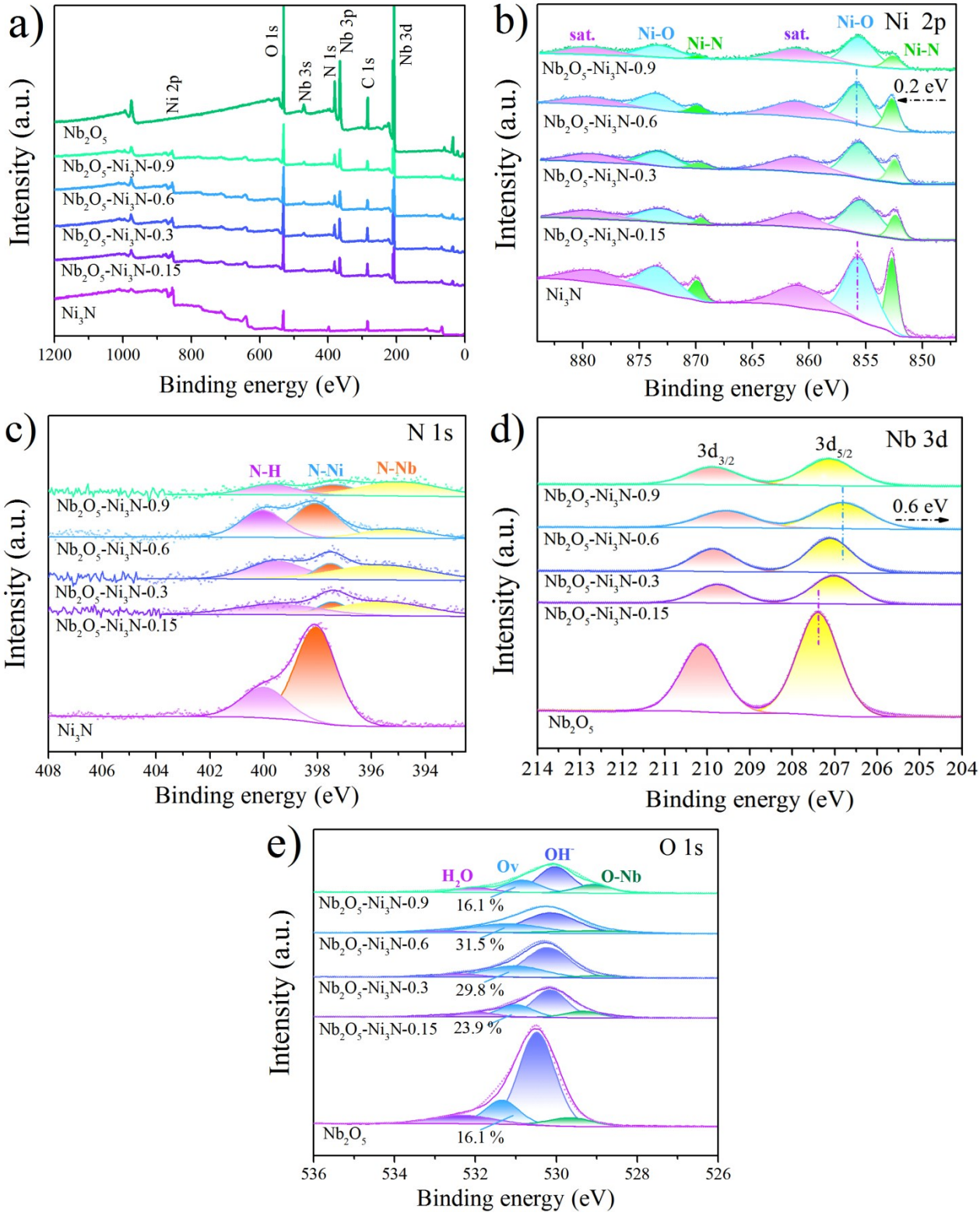

Fig. S8. a) The XPS spectra of Ni_3N, Nb_2O_5-Ni_3N-x (x = 0.15, 0.3, 0.6, 0.9) and Nb_2O_5, b-e) high resolution XPS spectra of Ni, N, Nb, and O, respectively.

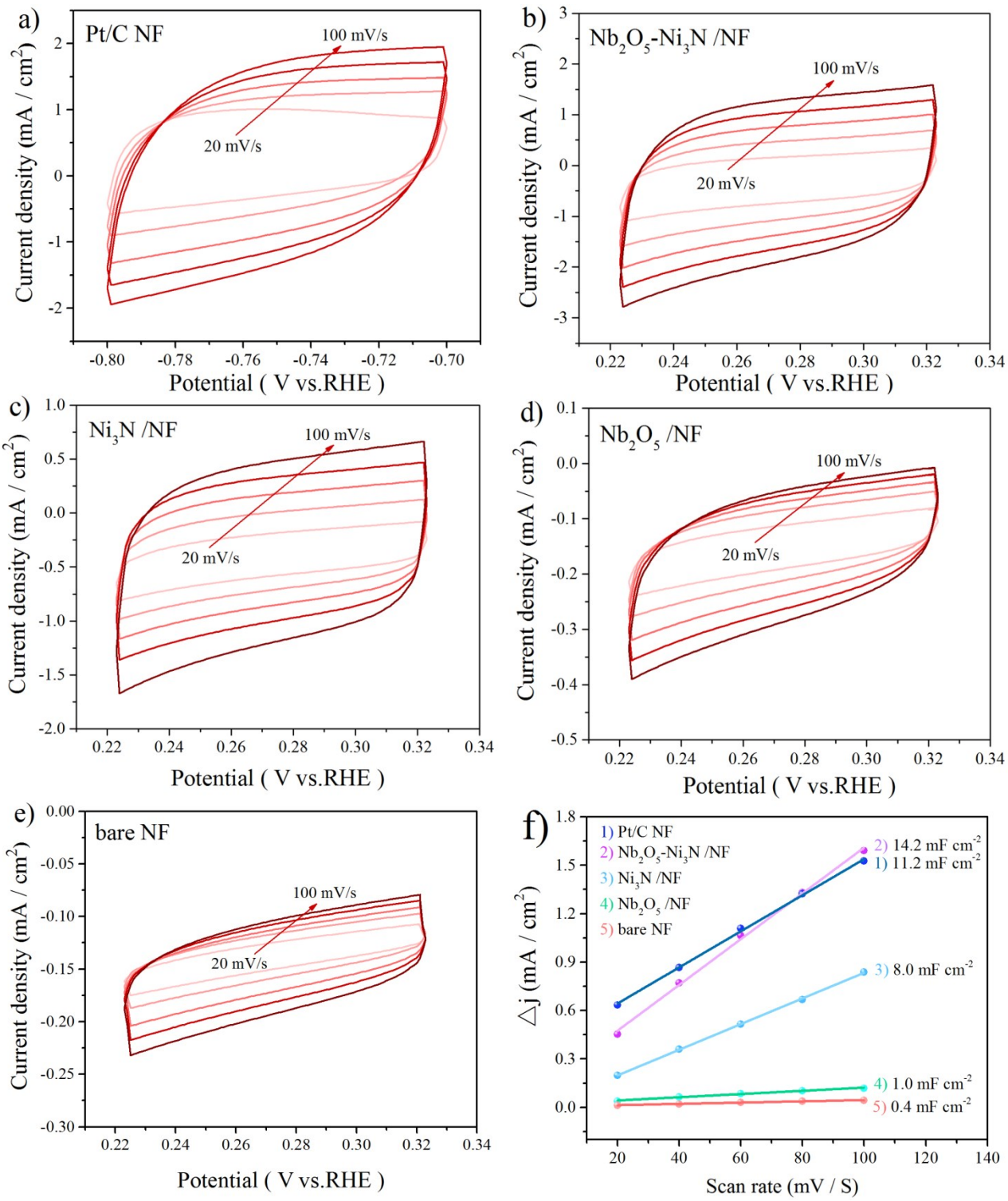

Fig. S9. CV curves of a) Pt/C/NF, b) Nb_2O_5-Ni_3N/NF, c) Ni_3N/NF, d) Nb_2O_5/NF, and e) bare NF measured in 1.0 M KOH solution at scan rates from 20 to 100 mV/s. f) The capacitive current at 0.27 V vs. RHE of the as-prepared catalysts.

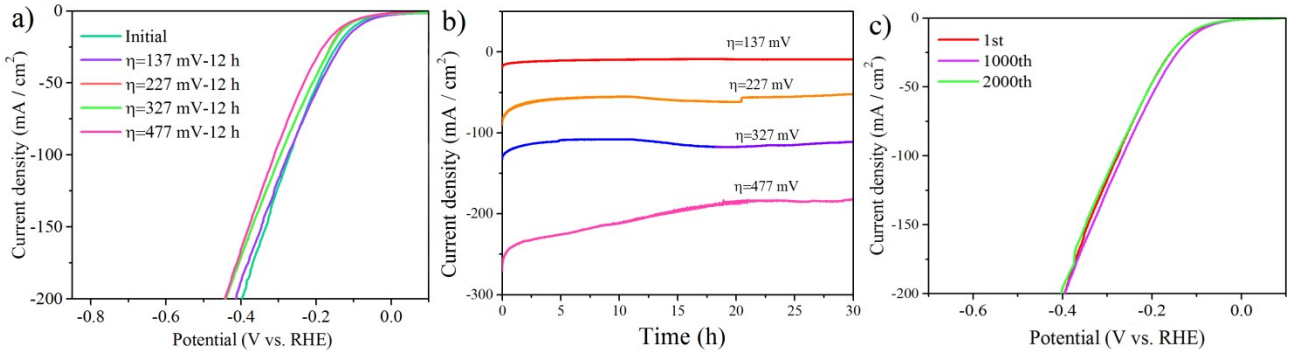

Fig. S10. a) LSV curves of Nb_2O_5-Ni_3N before and after a) 12 h of maintaining the overpotential at 137, 227, 327, and 477 mV, b) Chronoamperometry measurements of Nb_2O_5-Ni_3N under the various overpotentials for 30 h, c) LSV curves of Nb_2O_5-Ni_3N before and afte1000/2000 cycles of CV scanning.

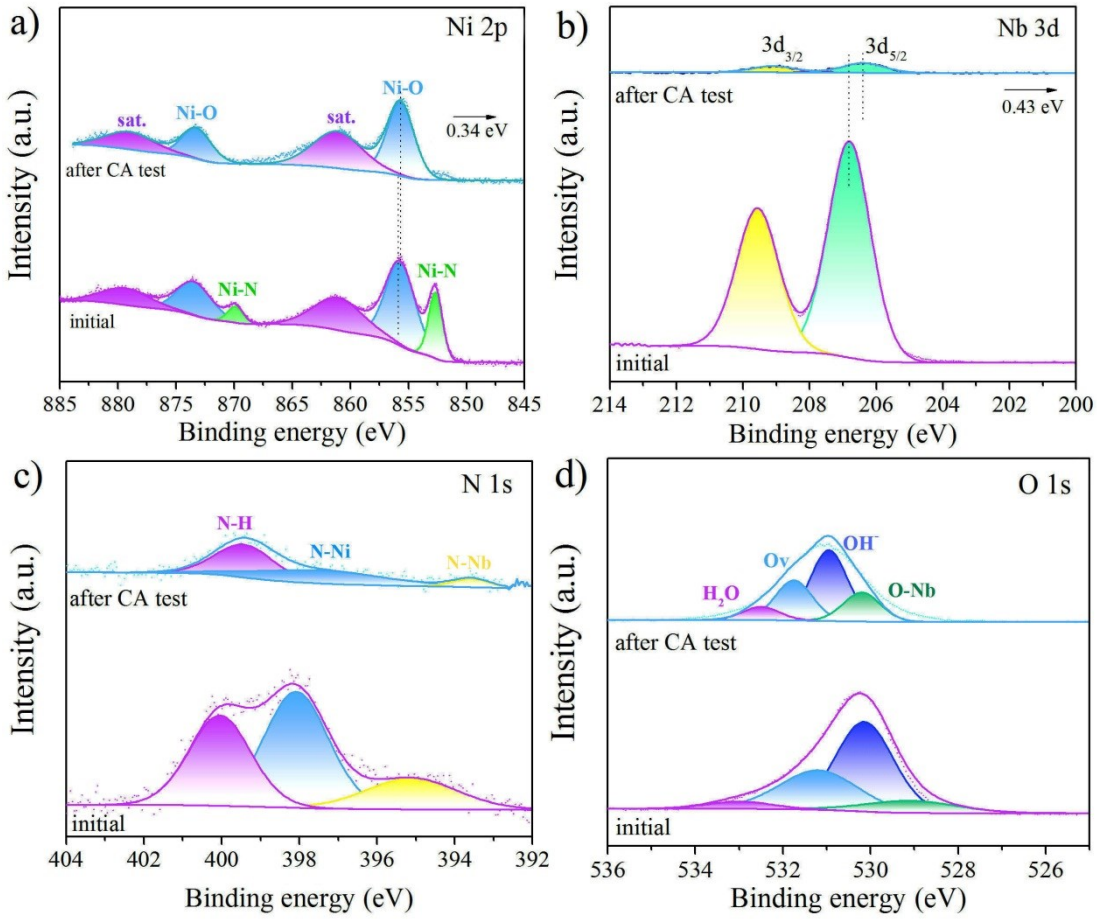

Fig. S11. Comparison of XPS analyses of Nb_2O_5-Ni_3N for a) Ni 2p, b) Nb 3d, c) N 1s, and d) O 1s before and after catalysis of the material.

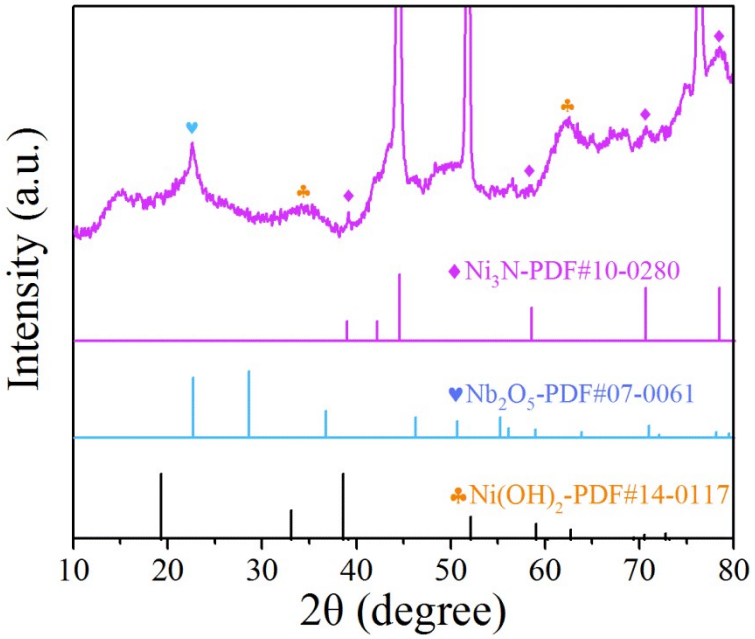

Fig. S12. XRD spectrum of Nb_2O_5-Ni_3N/NF after 48 h of stability test for HER in 1.0 M KOH.

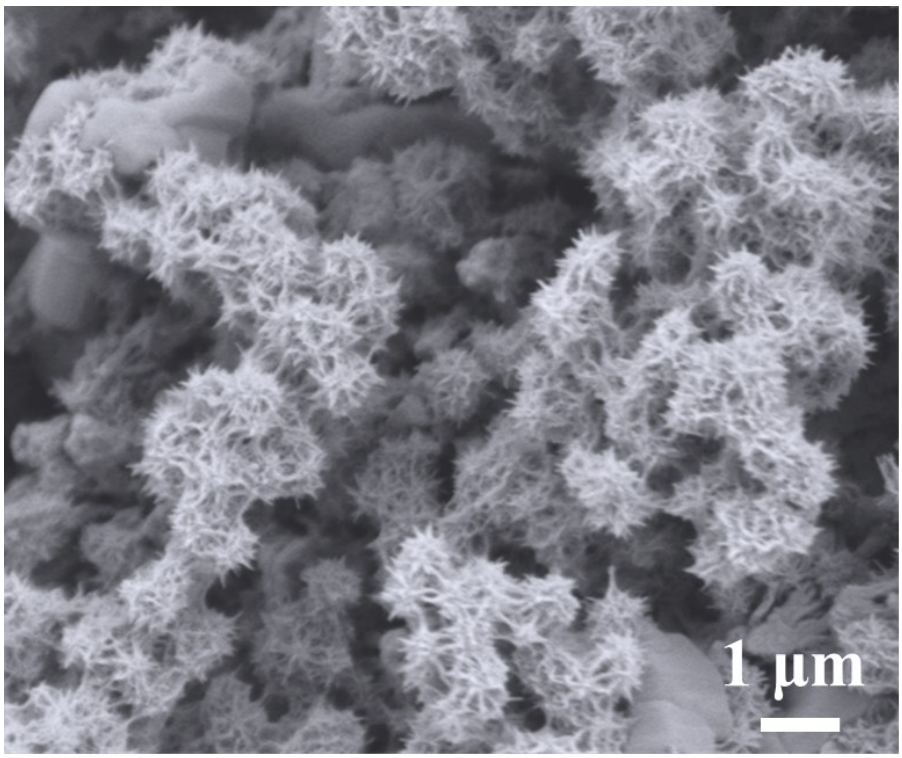

Fig. S13. SEM image of Nb_2O_5-Ni_3N after 48 h of stability test for HER in 1.0 M KOH

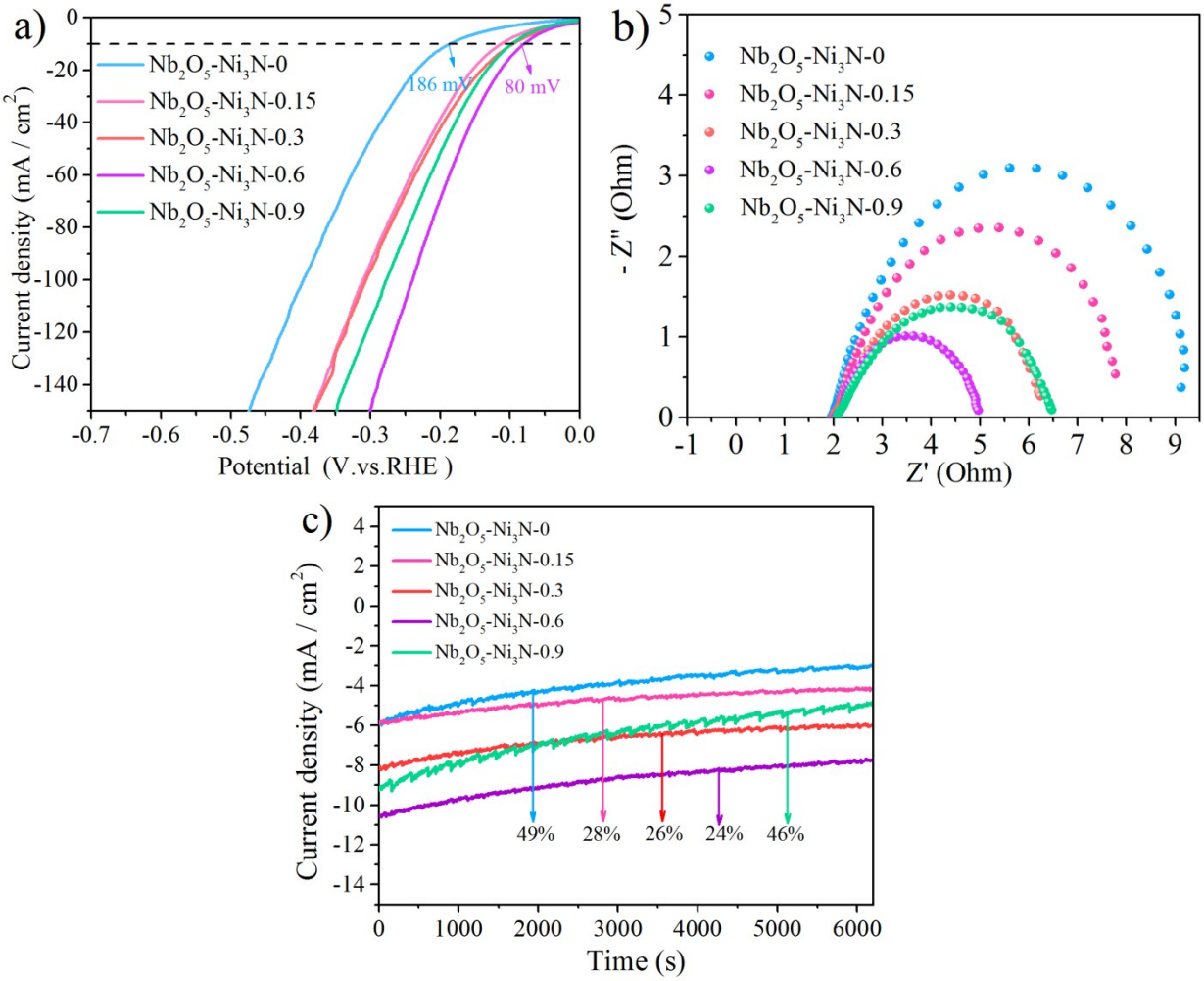

Fig. S14. a) LSV curves of Nb_2O_5-Ni_3N-x (x = 0, 0.15, 0.3, 0.6, and 0.9 mmol) in 1.0 M KOH solution; b) EIS Nyquist plots of the as-prepared catalysts; c) Chronoamperometry measurements of Nb_2O_5-Ni_3N-x at η = 137 mV.

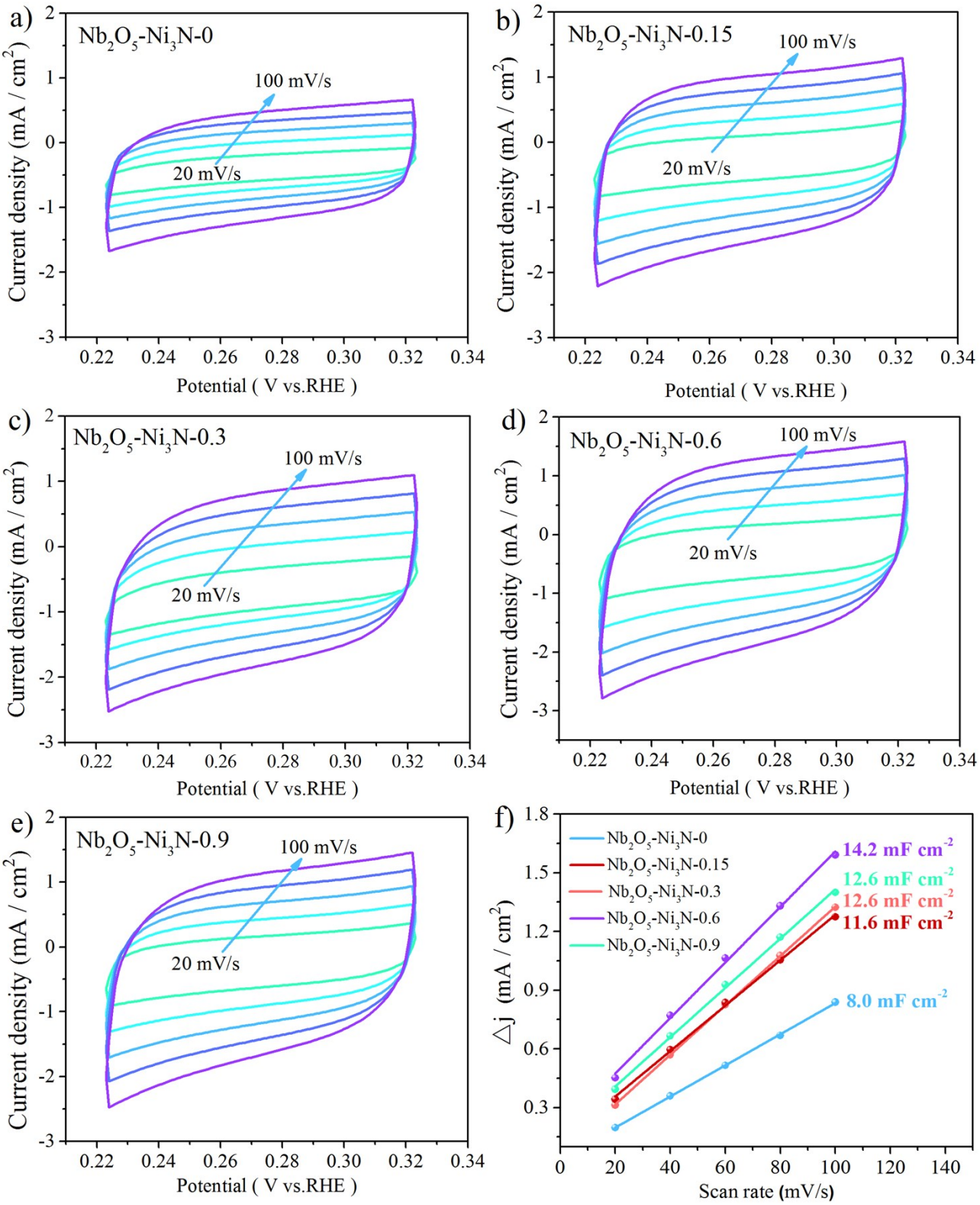

Fig. S15. CV curves of Ni_3N with different contents of Nb^{5+}: a) 0, b) 0.15, c) 0.3, d) 0.6, and e) 0.9 mmol measured in 1.0 M KOH solution at scan rates from 20 to 100 mV/s. f) The capacitive current at 0.27 V vs. RHE of the as-prepared catalysts.

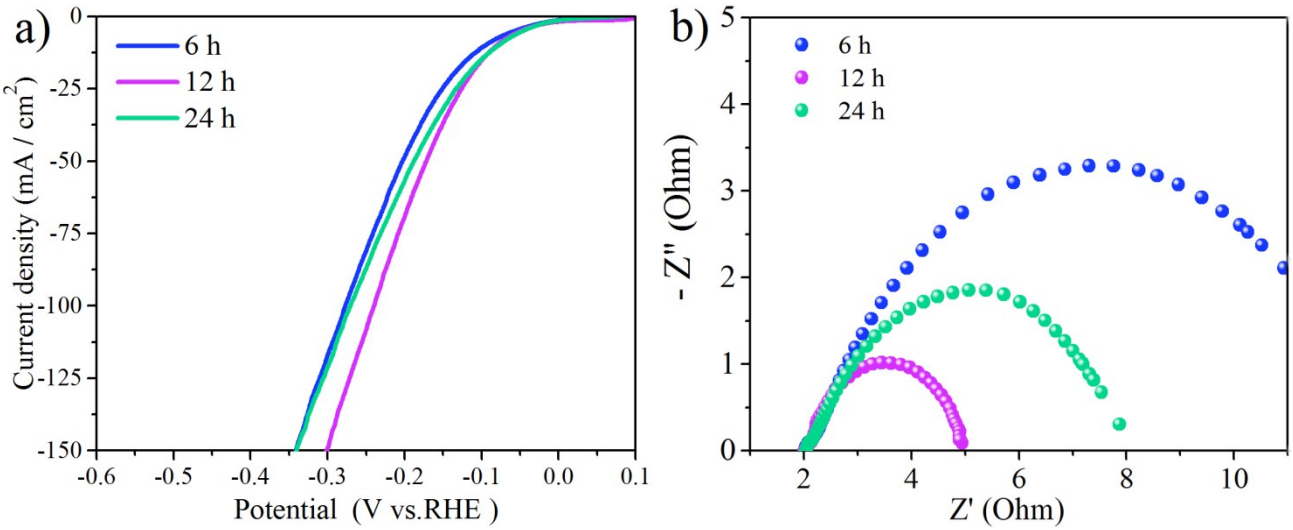

Fig. S16. a) LSV curves and b) EIS Nyquist plots of Nb_2O_5-Ni_3N at different hydrothermal reaction times.

.

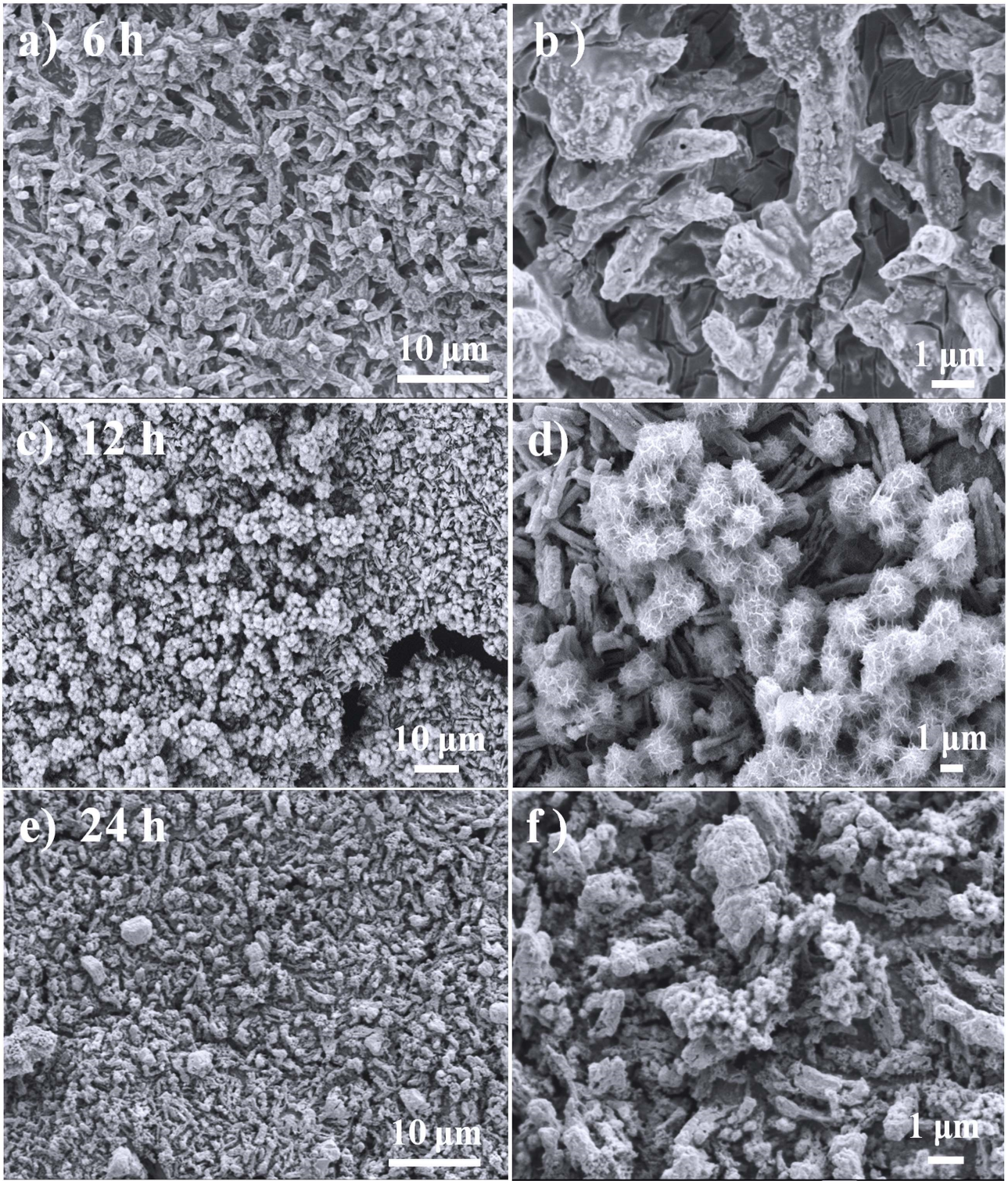

Fig. S17. SEM images of Nb_2O_5-Ni_3N prepared with different hydrothermal times: a-b) 6 h, c-d) 9 h, and e-f) 24 h.

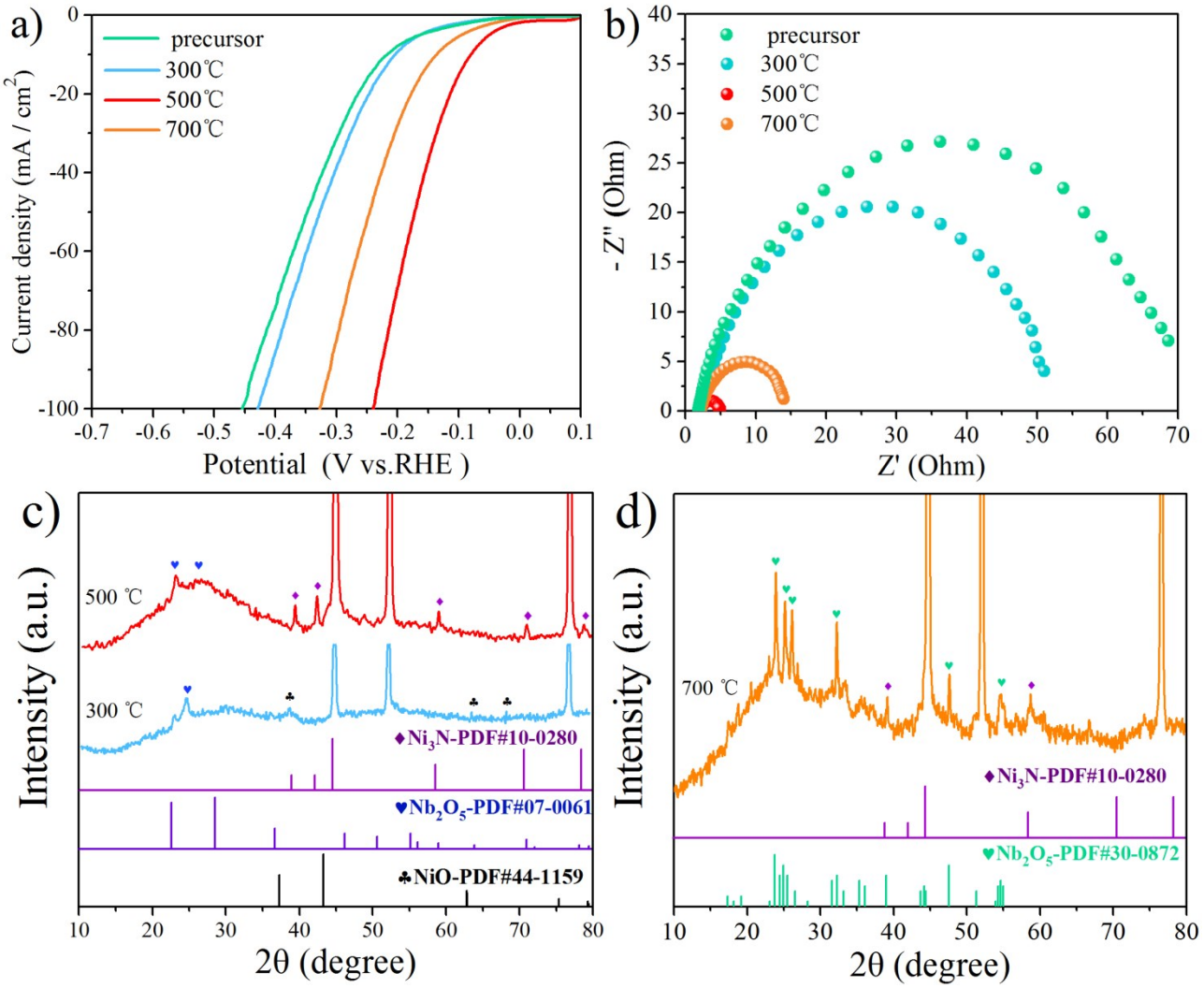

Fig. S18. a) LSV curves and b) EIS Nyquist plots of Nb_2O_5-Ni_3N at different nitridation temperatures; c-d) XRD patterns of the catalysts at different nitridation temperatures.

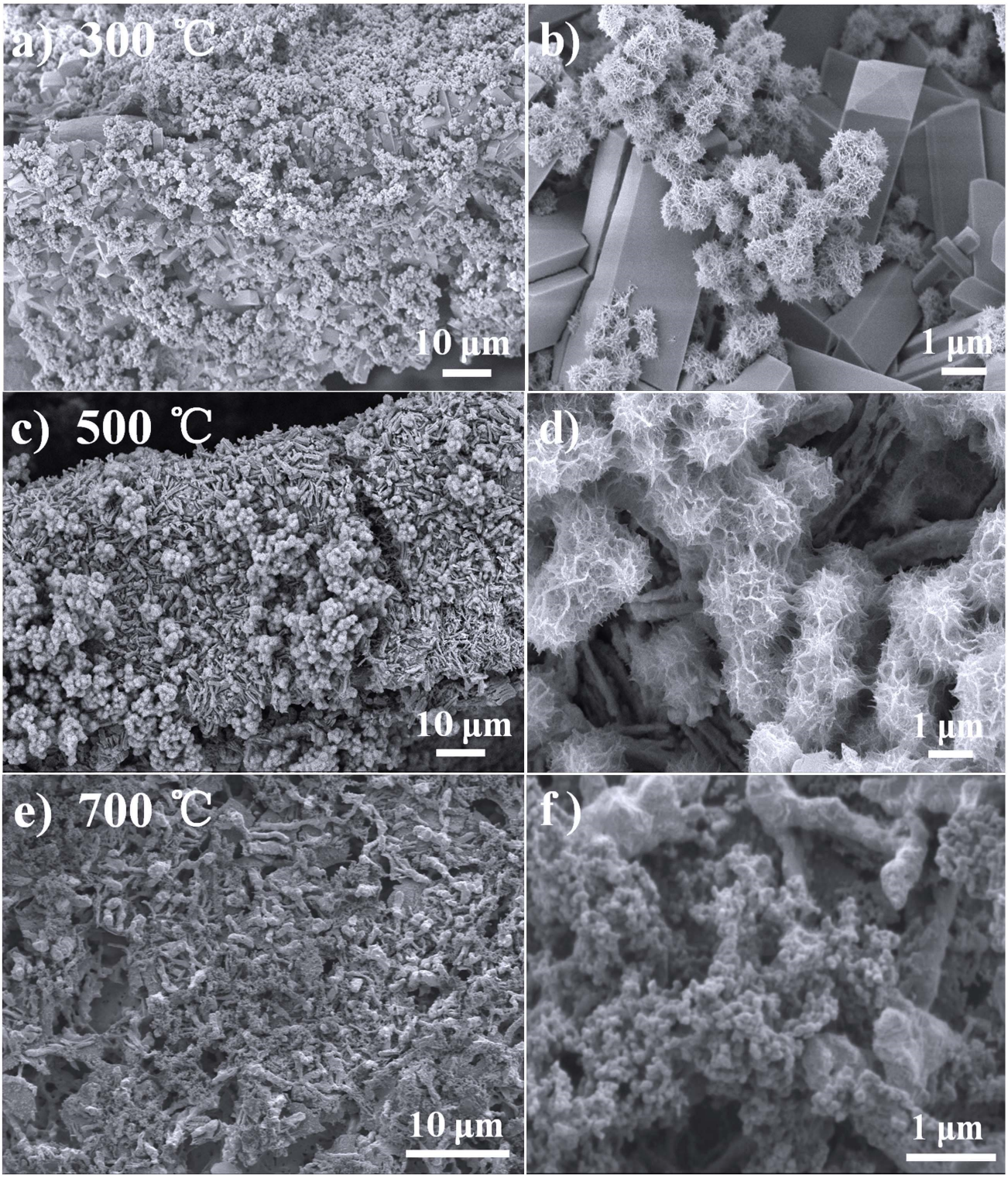

Fig. S19. SEM images of Nb_2O_5-Ni_3N prepared with different nitridation temperatures: a-b) 300 ℃, c-d) 500 ℃, and e-f) 700 ℃.

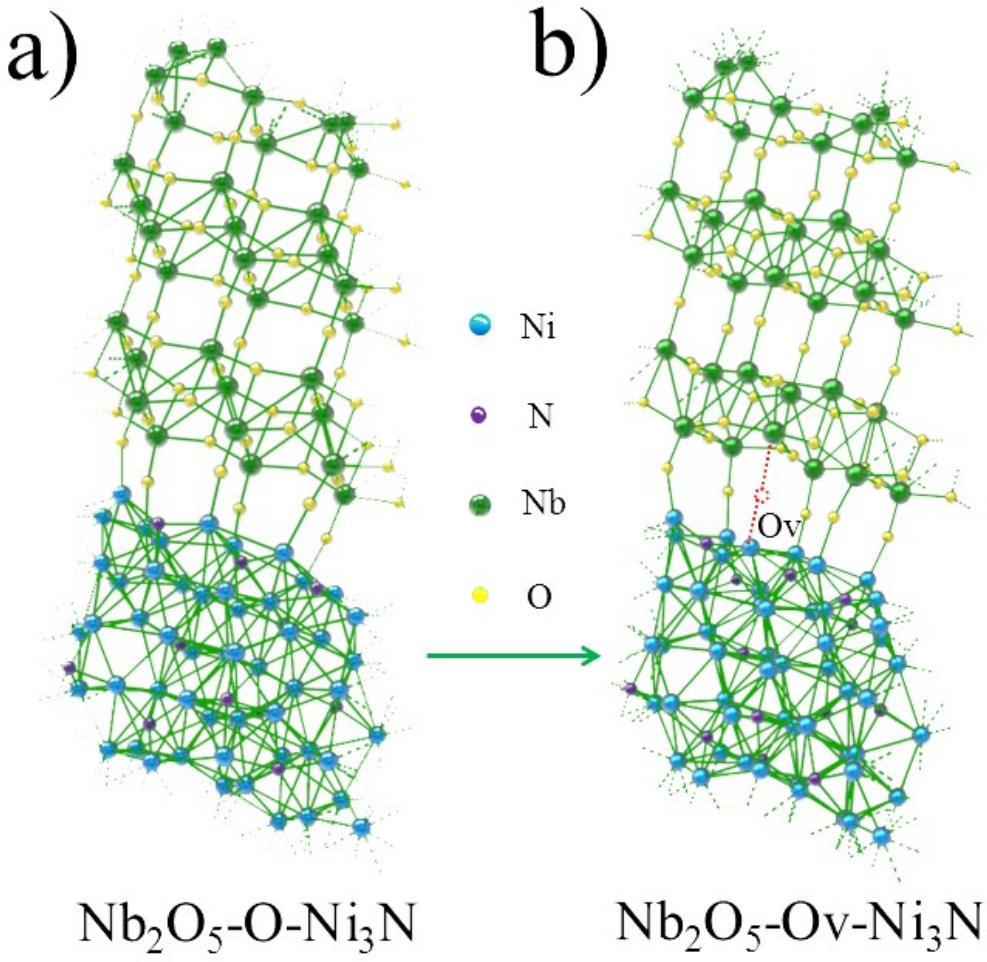

Fig. S20. Schematic model of Nb_2O_5-O-Ni_3N and Nb_2O_5-Ov-Ni_3N (O_v = oxygen vacancy). Without special instructions, Nb_2O_5-Ni_3N mentioned in the manuscript is Nb_2O_5-O_v-Ni_3N.

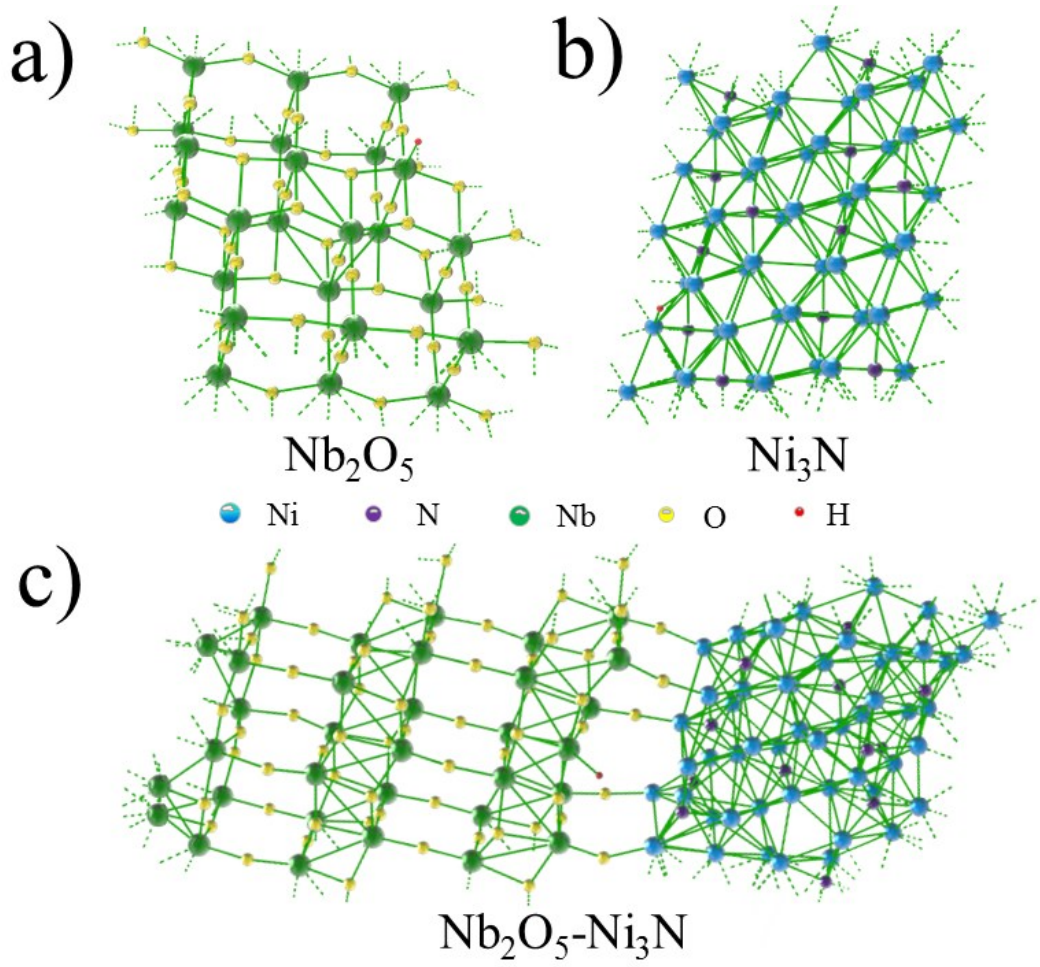

Fig. S21. Calculation models for adsorption of H* on a) Nb_2O_5, b) Ni_3N, and c) Nb_2O_5-Ni_3N.

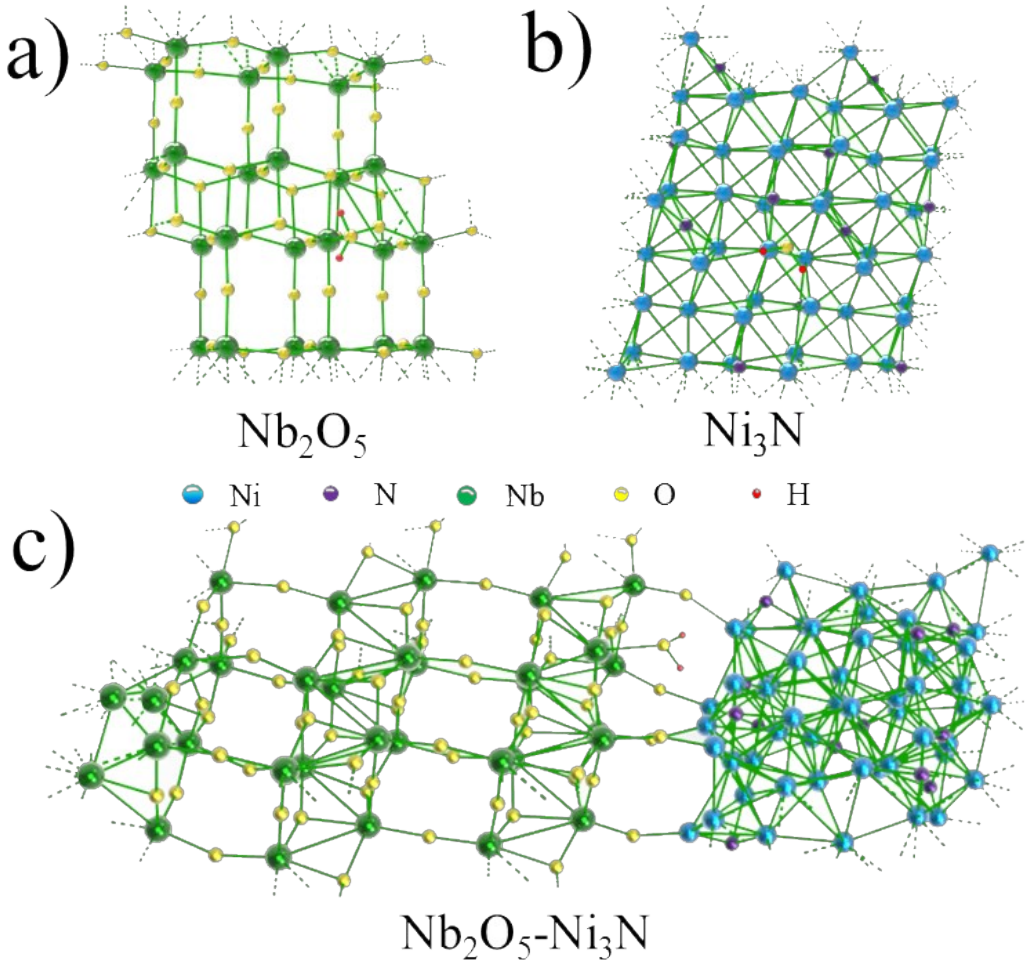

Fig. S22. Calculation models for H_2O adsorption on a) Nb_2O_5, b) Ni_3N, and c) Nb_2O_5-Ni_3N.

Table S1. Comparison of electrocatalytic activity for HER of this work with other non-noble catalysts in 1.0 M KOH solution.

Catalyst	Substrate	η_{10} (mV)	Reference
NiMoN	Ni foam	109	1
Ni_3N	glassy carbon	305	2
Co-Ni_3N	carbon cloth	194	3
Ni_3FeN	glassy carbon	158	4
NiMoN	carbon cloth	109	5
$NiCo_2N$	Ni foam	180	6
MoS_2-Ni_3S_2	Ni foam	98	7
$NiCo_2S_4$	Ni foam	210	8
MoS_2/NiFe-LDH[a]	glassy carbon	110	9
V-NiS_2	glassy carbon	110	10
$Ni_{1.5}Fe_{0.5}P$	Ni foam	128	11
NiCoP/rGO[b]	glassy carbon	209	12
Ni/NiO(OH)	rotating glassy carbon	190	13
NiO	carbon fiber	110	14
Nb_2O_5-Ni_3N	Ni foam	80	[This work]

a) LDH: layered bimetallic hydroxide. b) rGO: reduced graphene oxide.

Table S2. Comparison of stability data of Nb_2O_5-Ni_3N-x.

Catalyst	j_i (mA/cm^2)	j_t (mA/cm^2)	j_a (mA/cm^2)	Decrement/%
Nb_2O_5-Ni_3N-0	-5.9	-3.0	4.0	49
Nb_2O_5-Ni_3N-0.15	-5.8	-4.2	4.8	28
Nb_2O_5-Ni_3N-0.3	-8.1	-6.0	6.7	26
Nb_2O_5-Ni_3N-0.6	-10.5	-8.0	8.8	24
Nb_2O_5-Ni_3N-0.9	-9.1	-4.9	6.5	46

j_i: initial current density. j_t: termination current density. j_a: average current density.

Decrement = $(j_i - j_t) / j_i$

References

1 B. Chang, J. Yang, Y. Shao, L. Zhang, W. Fan, B. Huang, Y. Wu and X. Hao, *ChemSusChem*, 2018, **11**, 3198-3207.

2 D. Gao, J. Zhang, T. Wang, W. Xiao, K. Tao, D. Xue and J. Ding, *J. Mater. Chem. A*, 2016, **4**, 17363-17369.

3 C. Zhu, A. L. Wang, W. Xiao, D. Chao, X. Zhang, N. H. Tiep, S. Chen, J. Kang, X. Wang, J. Ding, J. Wang, H. Zhang and H. J. Fan, *Adv.Mater.*, 2018**, 30**, 1705516.

4 X. Jia, Y. Zhao, G. Chen, L. Shang, R. Shi, X. Kang, G. I. N. Waterhouse, L. Z. Wu, C. H. Tung and T. Zhang, *Adv. Energy Mater.*, 2016, **6**, 1502585.

5 Y. Zhang, B. Ouyang, J. Xu, S. Chen, R. S. Rawat and H. J. Fan, *Adv. Energy Mater.*, 2016**, 6**, 1600221.

6 Y. Wang, B. Zhang, W. Pan, H. Ma and J. Zhang, *ChemSusChem*, 2017, **10**, 4170-4177.

7 Y. Yang, K. Zhang, H. Lin, X. Li, H. C. Chan, L. Yang and Q. Gao, *ACS Catal.*, 2017**, 7**, 2357-2366.

8 A. Sivanantham, P. Ganesan and S. Shanmugam, *Adv. Funct. Mater.*, 2016, **26**, 4661-4672.

9 P. Xiong, X. Zhang, H. Wan, S. Wang, Y. Zhao, J. Zhang, D. Zhou, W. Gao, R. Ma, T. Sasaki and G. Wang, *Nano Lett.*, 2019, **19**, 4518-4526.

10 H. Liu, Q. He, H. Jiang, Y. Lin, Y. Zhang, M. Habib, S. Chen and L. Song, *ACS Nano*, 2017, **11**, 11574-11583.

11 H. Huang, C. Yu, C. Zhao, X. Han, J. Yang, Z. Liu, S. Li, M. Zhang and J. Qiu, *Nano Energy*, 2017, **34**, 472-480.

12 J. Li, M. Yan, X. Zhou, Z. Q. Huang, Z. Xia, C. R. Chang, Y. Ma and Y. Qu, *Adv. Funct. Mater.*, 2016, **26**, 6785-6796.

13 J. Ren, M. Antonietti and T. P. Fellinger, *Adv. Energy Mater.*, 2015, **5**, 1401660.

14 T. Zhang, M. Y. Wu, D. Y. Yan, J. Mao, H. Liu, W. B. Hu, X. W. Du, T. Ling and S. Z. Qiao, *Nano Energy*, 2018**, 43**, 103-109.